Nuclear Engineering and Design 321 (2017) 230–243

Contents lists available at ScienceDirect

Nuclear Engineering and Design

journal homepage: www.elsevier.com/locate/nucengdes

Mechanistic studies of single bubble growth using interface-tracking methods

Susann Hänsch [a,*], Simon Walker [a], Chidambaram Narayanan [b]

[a] Department of Mechanical Engineering, Imperial College London, Exhibition Road, London SW7 2AZ, United Kingdom
[b] Ascomp AG, Switzerland

HIGHLIGHTS

- Validation of a phase change model at the curved vapour-liquid interface.
- Analysis of different approaches for modeling the microlayer evaporation.
- Significance of conjugate heat transfer for microlayer evaporation.
- Role of evaporative thermal resistance for evaporation from the microlayer.
- Mechanistic simulation of the hydrodynamics of microlayer formation.

ARTICLE INFO

Article history:
Received 31 May 2016
Received in revised form 22 July 2016
Accepted 3 August 2016
Available online 20 August 2016

ABSTRACT

The growth of a vapour bubble at a heated surface involves various fluid mechanics, heat transfer and phase change phenomena. In this paper we present recent work under the auspices of the NURESAFE project aimed at developing mechanistic modelling of this. Evaporation at the curved surface of the bubble requires evaluation of the unsteady heat conduction within the surrounding liquid, coupled to an appropriate phase change model at the vapour–liquid interface. Issues around the development and implementation of such a phase change model are addressed. For low-pressure bubbles, however, a large fraction of the total evaporation takes place from the "microlayer"; a thin layer of water coating the heated substrate, which is left behind as the bubble expands. This microlayer evaporation requires careful, sub-grid modelling, as heat fluxes through the thin layer are very high. In particular, we demonstrate here the need both for modelling of the conjugate heat transfer within the substrate, and the importance of the incorporation of evaporative thermal resistance at the vapour–liquid interface. Despite the important role it plays in bubble growth, the mechanisms governing the formation, and resulting dimensions, of this microlayer are very little understood. We finish with a presentation of some early results attempting to investigate mechanistically the hydrodynamics of microlayer formation.

1. Introduction

A thorough understanding of the fundamentals of the boiling process on the scale of single bubbles is crucial for the further improvement of macroscopic boiling models. There is an emerging consensus about the various physical processes involved in the growth and the departure of steam bubbles from heated surfaces. Much effort has been applied to develop understanding and modelling capabilities for these processes, which can be incorporated into micro-scale simulations that allow detailed analysis of the growth of a single bubble.

Vapour generation during nucleate boiling is now known to occur in two different regions around the bubble as illustrated in Fig. 1.

Bubble growth is partly driven by evaporation from the bubble's curved surface, caused by a superheated liquid layer around the bubble, also termed the 'relaxation' layer. The ability to predict accurately the interphase mass transfer from such curved surfaces is essential for the simulation of any phase change phenomena using interface-tracking techniques.

The other mechanism is the evaporation of a thin layer of liquid beneath the steam bubble, which is termed the 'microlayer'. The microlayer can develop during the early stages of bubble growth, when the expanding bubble leaves behind a liquid layer a few microns thick between the heated wall and the underside of the bubble. Being all that separates the superheated wall from the

* Corresponding author.
E-mail addresses: s.haensch13@imperial.ac.uk (S. Hänsch), narayanan@ascomp.ch (C. Narayanan).

http://dx.doi.org/10.1016/j.nucengdes.2016.08.003
0029-5493/

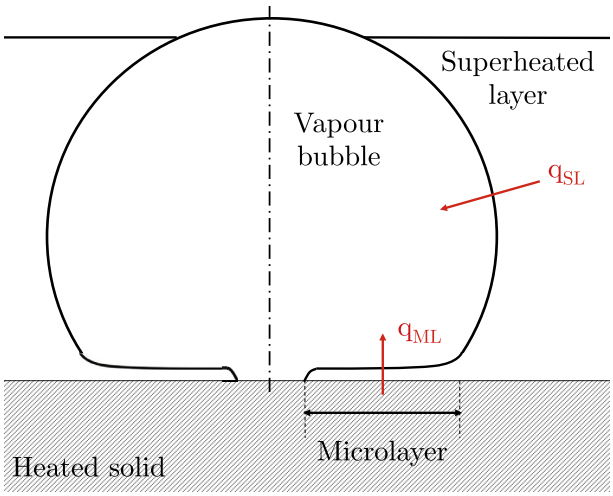

Fig. 1. Vapour generation mechanisms during bubble growth.

vapour, the microlayer evaporates rapidly and can contribute significantly to the bubble's growth.

The contribution of each of these evaporation mechanisms to the overall bubble growth is still debated in the literature and indeed their relative importance depends on the particular conditions that obtain. Table 1 lists typical physical parameters for steam bubbles measured in experiments at atmospheric pressure (Jung and Kim, 2015) and at a higher pressure (Sakashita, 2011). For high-pressure bubbles the bubble growth rate is generally much smaller than at atmospheric pressure with small departure diameters of ~100 μm for similar departure times. Microlayers are not observed at all and their contribution to vapour generation is believed to be minimal under high-pressure conditions (Sakashita, 2011). On the contrary, atmospheric pressure bubbles tend to be much larger by the time they depart, and during this growth do tend to leave microlayers beneath them, and the evaporation of these microlayers plays an important role in the growth and eventual departure of such bubbles.

This paper reports recent work under the NURESAFE project investigating the performance of various aspects of the modelling of mass transfer and bubble growth in interface-tracking CFD analysis of microscopic boiling.

Section 2 will focus on the evaporation from the curved surface. The approach used in this work in essence, by construction, takes the interface temperature to equal the saturation temperature at the relevant pressure, and models the rate of vapour generation as being determined by the heat flux to the interface from the superheated surrounding liquid. This heat flux is itself a consequence of the transient radial temperature gradient, as the temperature reduction propagates back into the bulk of the liquid.

In Section 3 we address the related but different issues associated with heat transfer through and mass transfer from the microlayer. In the literature there are two broad approaches, the "triple line" description of evaporation, and 'whole microlayer' models. We investigate these, and discuss recent improvements to the current state-of-the-art in microlayer mass transfer modelling. In particular, we will address the significance of conjugate heat transfer in the heated wall, and the role that evaporative resistance is believed to play in the microlayer region.

Despite their probably dominant role in much bubble growth, the mechanism for the formation of microlayers is little understood, and the modelling tends to be based upon empirical incorporation of very sparse experimental data. In Section 4 we present simulations of the hydrodynamics of microlayer formation during the very early stage of bubble growth. These simulations aim to add to the understanding of the underlying processes that lead to the formation of microlayers and the physical quantities governing their characteristics.

Conclusions and suggestions for possible future directions of research are presented in Section 5.

Table 1
Typical physical parameters for bubbles at atmospheric and high-pressure conditions.

Physical parameter	Atmospheric bubble	High pressure bubble
Pressure [MPa]	0.1	4.47
Departure diameters [mm]	~4	~0.1
Departure period [ms]	~20	10
Average growth rate [mm/s]	100	5
Observed microlayers	Yes	No

2. Macroscopic phase change model

2.1. Introduction

The physical phenomena of interfacial mass transfer, as it occurs in boiling or condensing flows, and the associated temperature distribution near the gas–liquid interface are areas of active research. In recent years, a number of different models have emerged that examine the nature of the liquid and vapour states, and the transition between them, from different points of view. In a macroscopic treatment of boiling, in which phases coexist, the boundary between them is usually idealized as a surface at which discontinuity in properties occurs. At a much smaller scale there is a region between the bulk phases in which the molecules exhibit a transition between vapour and the liquid properties. These different points of view led to the development of a number of different phase change models over the last decades.

With increasing computer power and use of CFD some of these phase change models have been successfully incorporated into interface tracking simulations, where phase change processes are described with the tools of continuum mechanics.

In this section the physical basis of a phase change model is described, followed by a discussion of its inclusion into the level-set code TransAT.

2.2. The physical basis

In microscopic boiling modelling, it is normal to begin with a tiny, but arbitrarily sized vapour 'seed'. In the 'relaxation' approach adopted here, this vapour is taken to be at the saturation temperature. At the beginning of the analysis the surrounding liquid is taken to be at a uniform temperature, at a few degrees of superheat.

The liquid–vapour interface is taken to be at the saturation temperature, and this causes a transient diffusive reduction in temperature to propagate into the liquid (not unlike the normal error function solution for a suddenly-imposed step change in surface temperature of a medium). This is indicated qualitatively in Fig. 2.

This is of course associated with a (high) heat flux from the superheated liquid towards the saturation-temperature interface, and this heat flux is taken to cause the generation of saturated vapour, with the rate given by the relationship

$$\dot{m}''_{vapour} = \frac{1}{h_{fg}} k_l \frac{\partial T}{\partial n} \tag{1}$$

Note that this approach (implicitly) treats the actual process of evaporation at the surface as 'perfect', in that it offers no impediment to the vapour generation. We will return to this point shortly.

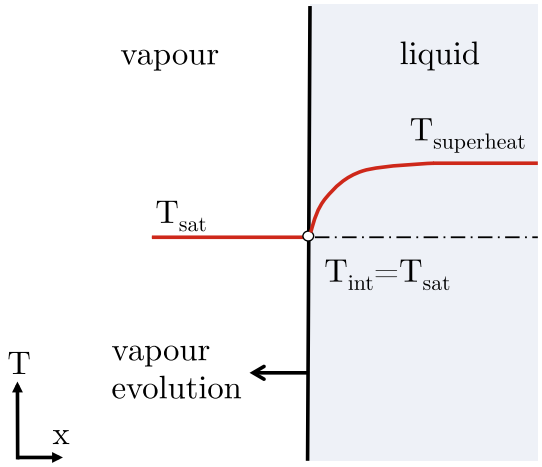

Fig. 2. The temperature distribution associated with the relaxation model.

In that this vapour generation rate causes the bubble to grow, the interface itself is thereby moved bodily. In addition, there is some motion of the interface caused by the loss of liquid mass corresponding to the gain of vapour mass.

For an atmospheric pressure bubble, over a typical growth time of ~20 ms as given in Table 1, the characteristic penetration depth of the temperature disturbance, taken as $\delta \sim \sqrt{\pi kt/\rho c_p}$, is ~100 μm. This is associated with an interface motion, from the bubble growth, of ~2000 μm, and a depth of liquid loss, to provide the vapour so generated, of less than ~1% of this motion.

The corresponding figures for a high-pressure bubble, according to Table 1, are a penetration depth of ~70 μm and an interface motion of only ~50 μm.

2.3. Computational implementation

In the level-set framework the spatial distribution of the phases is identified via a smoothed Heaviside function and physical properties in the interface cells are computed as an approximation of the properties of both fluids.

Recall, we would like the interface cell, that is, the cell by definition that lies between wholly liquid and wholly gas cells, to be at the (known) saturation temperature.

By an iterative process, the rate of mass transfer (in principle either condensation or evaporation) that is "asserted" to be occurring in the interface cell is adjusted, and the corresponding energy source or sink term calculated. This term is then used in the normal solution of the energy equation, and the interface cell temperature is computed. This process is repeated iteratively, until an interface temperature equal to the saturation temperature is computed.

The code computes the temperature distribution (the "error function shape") in the near-interface liquid region surrounding the vapour via solution of the usual energy equation as part of the ordinary CFD treatment.

The details are rather complex, but the outcome in principle provides a reasonable measure of the local rate of vapour generation, expressed as a volumetric source term and applied to the cell through which the interface passes. More details of the modelling scheme in general are available in (ASCOMP, 2015).

2.4. Comparison of the TransAT solution with an analytical solution

The phase change model is here tested by simulating the growth of a spherical bubble in an infinite superheated liquid. The work of Scriven (1959) provides an essentially exact analytical solution of the above model.

We address the case characterised by the values in Table 2. The working fluid is water at atmospheric pressure and the degree of superheat is 5 K.

The simulation was performed using an axisymmetric domain of 0.4 × 0.4 mm in radial extent and height. An initial vapour seed was placed in the domain surrounded by an initial thermal boundary layer, with the initial conditions provided by evaluation of the analytical solution (Scriven, 1959).

The water bubble starts with a seed of a radius of 30 μm and an initial thermal boundary layer thickness of (only) 2.3 μm thick. For the purpose of a grid dependency study three different uniform grids are used, as listed in Table 3.

Fig. 3 shows the predicted bubble radius over time for the different grid resolutions. The results are in qualitative agreement, but have large quantitative discrepancies with respect to the analytical solution. In particular they do not appear to exhibit convergence upon grid refinement for the grids simulated.

The challengingly small thermal penetration depth, consequent on the physical properties of water, is difficult to resolve sufficiently. A finer grid is required for accurate resolution of the thermal boundary layer, but very fine grids introduce a new problem with surface tension related parasitic currents that start to corrupt the solution upon grid refinement. Fig. 4 demonstrates the presence of these parasitic currents for the finest grid. The uneven temperature distribution shows that the interface temperature is not kept at the saturation temperature.

2.5. Investigation into convergence behaviour

A less challenging fictitious fluid is characterised in Table 4. The fictitious fluid is chosen to have a higher thermal diffusivity so as to make the thermal boundary layer thicker and therefore easier to resolve.

For the case of the fictitious fluid the vapour seed has a radius of 300 μm and a thermal boundary layer thickness of 312 μm. The characteristics of the meshes used to analyse bubble growth in this fictitious fluid are given in Table 5. Results of the simulations are presented in Fig. 5.

The bubble growth results in Fig. 5 are both in qualitative and quantitative agreement and exhibit convergence upon grid refinement.

In Fig. 6 the observed bubble shape and temperature distribution around the bubble are illustrated. For this test case the bubble is able to keep its spherical shape. The vapour temperature inside the bubble is uniformly at saturation and the interface temperature stays at the saturation value.

2.6. Discussion

In summary, for cases with high phase change rates under conditions of large density ratios between the vapour and the liquid, and low liquid thermal diffusivity, the thermal boundary layer resolution demands very small cell sizes.

Table 2
The physical properties for water at 1 bar.

Test case	Water at 1 bar	
Physical property	Liquid	Vapour
σ [N/m]	0.0589	
h_{lv} [kJ/kg]	2257	
T_{sat} [K]	373.15	
ρ [kg/m^3]	958	0.579
μ [μPa · s]	277	12.55
c_p [J/kgK]	4220	2030
λ [W/mK]	0.679	0.025

Table 3
Mesh characteristics for the Scriven test cases.

Test case	Water at atmospheric pressure		
Grid	Element number	Δx [μm]	Nodes in thermal boundary layer
Coarse	200 × 200	2	1
Mid	400 × 400	1	2
Fine	800 × 800	0.5	4

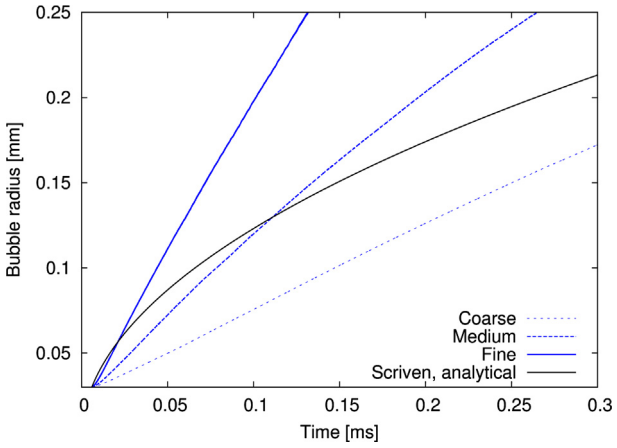

Fig. 3. The bubble growth using the relaxation model for water at atmospheric pressure.

As is seen, the predictions are all better, and show the expected convergence characteristics, for the fictitious fluid used to explore this. The poorer convergence behaviour in the more challenging case of water under atmospheric pressure is under active investigation.

In order to obtain accurate solutions at reasonable grid sizes, second-order heat-flux models are needed to calculate the temperature gradients, such as the sharp-interface method suggested by Gibou et al. (2007). The sharp-interface method has already been incorporated into TransAT and validated with the Scriven test case for a one dimensional treatment (corresponding to the assumption of spherical symmetry) (Guion et al., 2013b). The further development of the sharp-interface method and its implementation in the three-dimensional code is part of ongoing work.

3. Modelling phase change in the microlayer

3.1. Introduction

Thin layers of liquid are known to be 'left behind' beneath essentially the entire extent of bubbles that grow rapidly at low pressures on heated substrates. The formation of these 'microlayers' has been well established by experimental observations. The work of Snyder and Edwards (1956) was the first to hypothesize the existence of thin liquid layers which evaporate rapidly, drawing substantial amounts of heat from the surface underneath growing bubbles. Later Moore and Mesler (1961) were able to provide qualitative verification of the existence of such microlayers by measuring temperature fluctuations on the surface underneath steam bubbles. In the following years other authors attempted to

Table 4
The physical properties for the fictitious fluid.

Test case	Fictitious fluid	
Physical property	Liquid	Vapour
σ [N/m]	0.1	
h_{lv} [kJ/kg]	100	
T_{sat} [K]	500	
ρ [kg/m^3]	200	5
μ [Pa · s]	0.1	0.005
c_p [J/kgK]	400	200
λ [W/mK]	40	1

Table 5
Mesh characteristics for the fictitious fluid Scriven test case.

Test case	Fictitious fluid		
Grid	Element number	Δx [μm]	Nodes in thermal boundary layer
Coarse	54 × 54	160	2
Mid	108 × 108	80	4
Fine	216 × 216	40	8

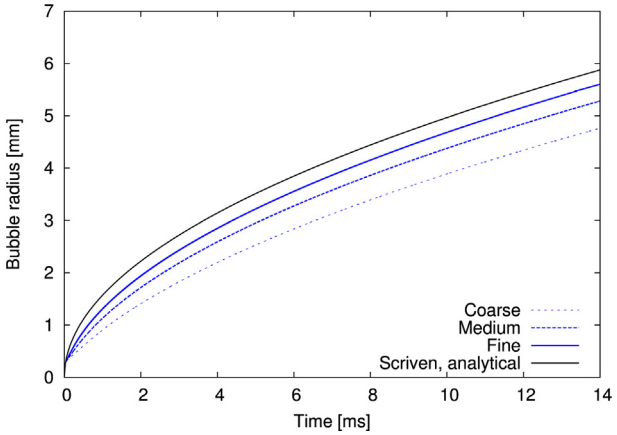

Fig. 5. The bubble growth using the relaxation model for the fictitious fluid.

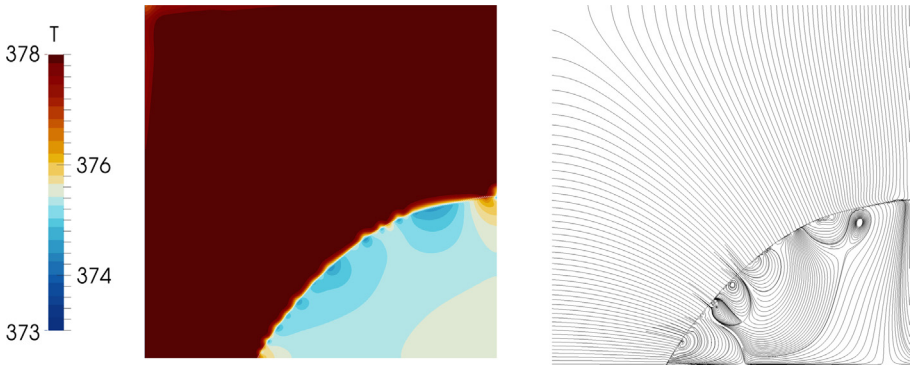

Fig. 4. Bubble shape, temperature distribution and streamline plot for the Scriven case after 0.1 ms (fine grid, entire domain).

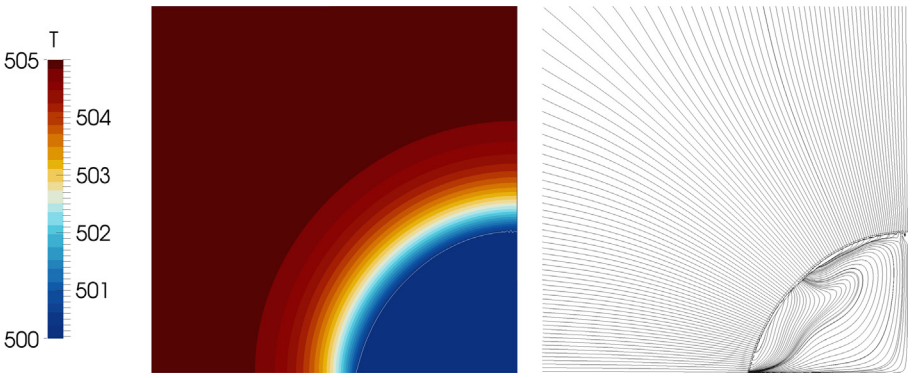

Fig. 6. Bubble shape, temperature distribution and streamline plot for the fictitious fluid case after 5 ms (fine grid, entire domain).

measure the thickness of this microlayer by interferometry, and using temperature–time measurements of the surface (Sharp, 1964; Cooper and Lloyd, 1969; Fath and Judd, 1978).

More recent experimental investigations (Koffmann and Plesset, 1983; Kim and Buongiorno, 2011; Yabuki et al., 2013; Jung and Kim, 2014) have generated a consensus picture of microlayers at atmospheric-pressure steam-water conditions. Their typical radial extension is about 1 mm, with maximum thicknesses measured between 1 and 5 μm (Koffmann and Plesset, 1983; Kim and Buongiorno, 2011; Yabuki et al., 2013; Jung and Kim, 2014). A schematic representation of the microlayer is shown in Fig. 7. Once it has formed, its evaporation rapidly cools the solid surface underneath, and the consequent conjugate heat transfer into the substrate strongly affects the process of microlayer evaporation (Hänsch et al., 2015). It is generally observed that microlayers are formed at high bubble growth rates (or equivalently with high wall superheats). At low superheats or high pressure conditions microlayers are observed less or not at all.

The contribution of the evaporation from the microlayer to bubble growth is still debated in the literature. Utaka et al. (2014) suggest that the contribution of the microlayer to bubble growth depends mainly on the superheat of the surface. From their experiments they concluded that different superheats (theirs ranged from 6 to 39 K) lead to entirely different microlayer contributions, ranging from 15% to 70% to the bubble volume. Generally, it is observed that microlayers are more important for bubbles growing with higher superheats.

We will here address three of the major aspects of microlayer analysis, that have featured in the NURESAFE activity: (i) The use of 'triple line or 'whole microlayer' models for computing evaporation, (ii) an investigation into the significance of transient conjugate heat transfer in the substrate, and (iii) the probable particular importance of evaporative thermal resistance in the context of microlayers.

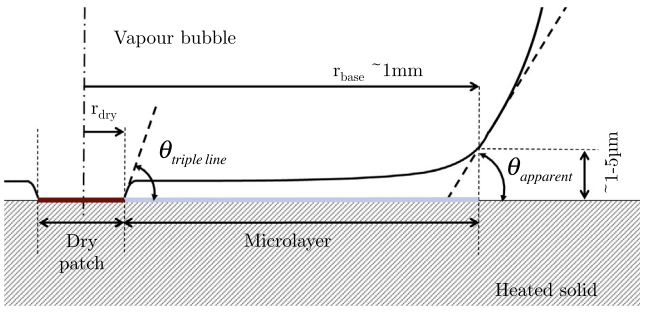

Fig. 7. Microlayer configuration under atmospheric pressure conditions (Hänsch and Walker, 2016b).

3.2. Triple line versus 'whole microlayer' models

The effect of microlayer evaporation is incorporated into CFD boiling analysis via semi-empirical 'sub-grid scale' modelling. Two different approaches have emerged in the literature to describe the evaporation mechanism from the underside of the bubble.

Early works focus on the modelling of the enhanced mass transfer at the so-called triple line, where all three phases coincide. The area covered draws a 'circle' rather than a 'disc' on the heated wall. More recent developments tend to use 'whole' microlayer models, which describe the evaporation from the entire radial extent of observed liquid microlayer. Both triple line and whole microlayer models have been incorporated into interface-tracking codes for the simulation of nucleate boiling phenomena. The intention of the next section is to investigate the relative merits of these two approaches as a model to describe the processes believed to be under way.

3.2.1. Triple line models

Triple line models address the circular line where the curved surface of the bubble intersects the heated surface, typically focusing on a very short region extending for about 1 μm radially outwards. As illustrated in Fig. 8, from a macroscopic perspective here all three phases appear to co-exist. However, the contact between the vapour-liquid interface and the solid is only apparent. It is thought (Wayner et al., 1976) that the dryout region is itself coated with a very thin (~1 nm) film of water molecules, adhering strongly to the metal surface. Due to the small thickness of the liquid film within the triple line region, for a long time it has been assumed that great heat fluxes exist in that region. For this reason, early works considered the accurate modelling of the triple line region a crucial component of any nucleate boiling simulation.

Modelling the flow and the heat transfer in the vicinity of triple lines has been a research area for several decades. The work of Wayner et al. (1976) was an early example, postulating that a capillary meniscus is connected to the adsorbed film. A large number of authors have since attempted to model this transition region (Moosman and Homsy, 1980; Wang et al., 2007, 2008; Stephan and Busse, 1992).

The modelling of the triple line in the literature may broadly be summarized as follows:

Typically the radial extent of the triple line region, even though very small (~1 μm), is still much larger than the maximum film thickness (~100 nm) in that area. Therefore, lubrication theory applies, allowing the formulation of a mass balance within the liquid wedge.

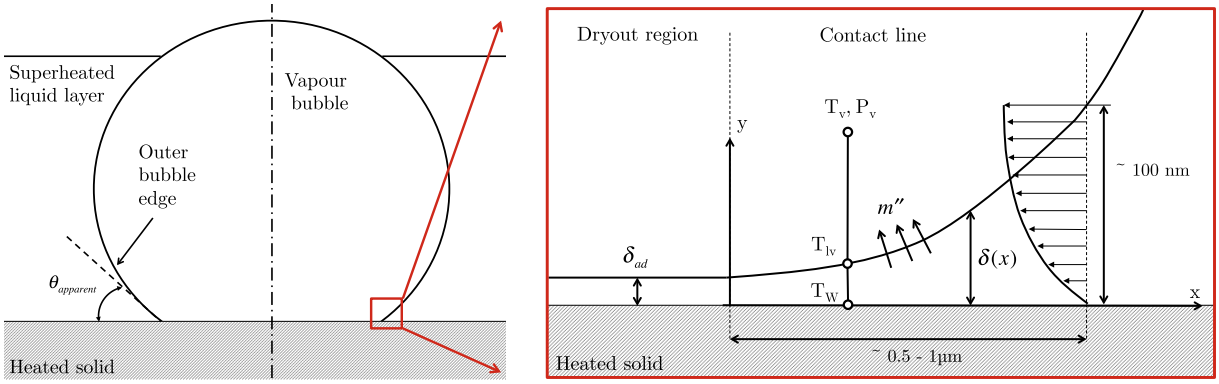

Fig. 8. Schematic of triple line models.

The pressure difference between vapour and liquid across the interface is described by the Augmented Young–Laplace Equation and arises from both capillary and disjoining pressure.

The heat within the triple line region is transferred by thermal conduction through the liquid, and via evaporation at the liquid–vapour interface:

$$q''(x) = m''(x)h_{fg} = \frac{k_l(T_W - T_{lv}(x))}{\delta(x)} = \frac{(T_W - T_{SAT})}{\frac{\delta(x)}{k_l} + \frac{1}{h_{evap}}} \quad (2)$$

Knowledge of the interface temperature $T_{lv}(x)$ is required. The assumption of a fixed temperature equal to the vapour saturation temperature is only applicable at relatively low heat fluxes (Langewisch, 2012). For liquid film thicknesses around 1 nm, as in the triple line region, predicted heat fluxes are much higher than those observed in experiments. Building on the kinetic theory (Schrage, 1953), for small film thicknesses the evaporative thermal resistance becomes a major constraint on mass transfer. Kinetic effects limit the mass and heat transfer rates, resulting in an increase of the interface temperature above the saturation value in the case of evaporation. Expressions for the interface temperature have been developed based on considerations on a molecular scale. In practice, the evaporative resistance is usually expressed in the form of an evaporative heat transfer coefficient. Several variants of such interface resistance models exist, all being based on the theory of Schrage (1953).

All considerations regarding mass, momentum and energy within the triple line region comprise a closed system of differential equations. These can be summarized into a single, highly nonlinear, 4th order ordinary differential equation for the thickness of the liquid wedge. For the solution of this equation authors have applied different strategies leading to different models for the enhanced evaporation from the triple line region.

One of the earliest applications of a triple line model to the analysis of nucleate boiling was by Stephan and Hammer (1994). Since then several numerical studies have included triple line models for the increased mass transfer underneath steam bubbles (Lay and Dhir, 1995; Son et al., 1999; Fuchs et al., 2006; Kunkelmann and Stephan, 2009). Some of these studies slightly misleadingly refer to the incorporated model for the enhanced evaporation underneath the bubble as a microlayer model. However, these models do not capture the entire radial extent of microlayer evaporation as it is observed in experiments.

3.2.2. Whole microlayer models

Microlayer models start from the experimental observation that a long, almost flat and very thin liquid layer of significant radial extent is observed beneath steam bubbles. It extends from the bubble nucleation site to the outer edge of the bubble base. The microlayer height is thinner towards the centre and increases gradually with radius, as illustrated in Fig. 9.

The modelling of microlayer evaporation has been studied for several decades. The basic model was originally suggested by the pioneering work of Cooper and Lloyd (1969), who also confirmed the existence of microlayers by temperature measurements at the heater surface. Since then the basic microlayer evaporation model has not changed greatly, and has been used in numerous works (Delgoshaei, 2009; Guion et al., 2013a; Utaka et al., 2013).

The more recent works of Chen and Utaka (2015) and Sato and Ničeno (2015) were the first to incorporate a microlayer evaporation model into interface-tracking codes. The successful simulation of the growth and departure of single bubbles from a heated surface has been demonstrated using a 'sub-grid' model for microlayer evaporation. A similar model has been implemented into the interface-tracking code TransAT and will be investigated in the following sections.

For the microlayer evaporation model a number of simplifying assumptions are made:

Since the liquid film is almost flat, the curvature of the gas–liquid interface is assumed to be negligible. Therefore, there is assumed to be no capillary pressure acting upon the liquid film over its entire radial extent.

The disjoining pressure, arising from attractive forces between molecules in the fluid and in the solid, is negligible. These forces typically act in the range of a few molecular diameters (in the case of water of the order of 0.275 nm), and therefore, can be safely neglected.

The gas–liquid interface is assumed to have no evaporative thermal resistance (contrary to the triple line models discussed above). Therefore, the interface temperature is fixed at the saturation temperature ($T_{\text{int}} = T_{SAT}$). (We will return to this point in Section 3.4.)

Under these assumptions the liquid pressure is equal to the vapour pressure and there is no lateral flow within the microlayer. Evaporation takes place, driven by heat conduction through the liquid layer from the solid substrate beneath. This provides some of the vapour that drives the bubble growth. The radial extent of the microlayer grows as the bubble expands. Once a fresh portion of the microlayer has been formed by the growth of the bubble, no further liquid is believed to flow into the layer along the surface. Rather, as evaporation takes place the microlayer becomes thinner. Evaporation eventually reduces the thickness to the adsorbed layer thickness, and as this occurs first at the slightly thinner, and 'older', radially-inboard end, the consequence is a hot dry patch in the centre of the bubble that grows in radius over time. Thus, the radial expansion of the dryout region becomes a direct consequence of microlayer evaporation.

If we consider the control volume in Fig. 9 at one particular radial location within the liquid film, the local evaporative mass

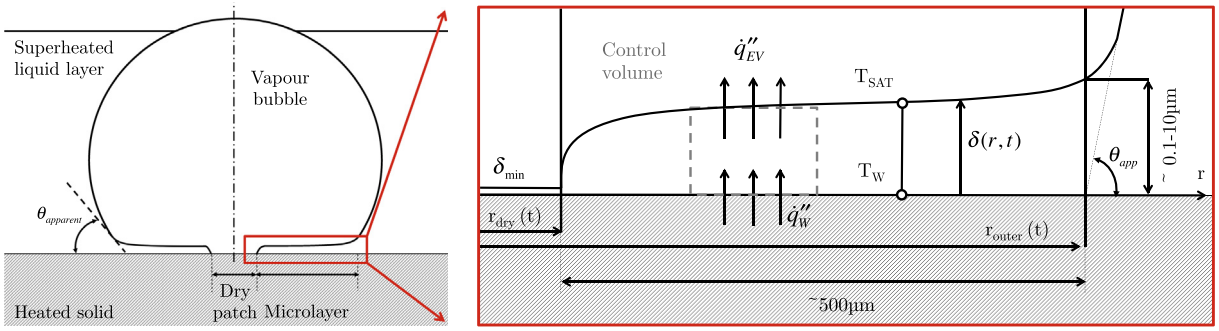

Fig. 9. The general picture of the microlayer region and schematic of a microlayer model.

flux can be simply described by the change in film height over time:

$$-\dot{q}''_{eV} = -\dot{m}''_{eV} h_{fg} = -\rho_l \frac{\partial \delta}{\partial t} h_{fg} \tag{3}$$

The corresponding conductive heat flux through the liquid film can be formulated as:

$$\dot{q}''_{eV} = \frac{k_l (T_W - T_{\text{int}})}{\delta(r,t)} \tag{4}$$

By eliminating the evaporative heat flux from the equations above, the time evolution of microlayer thickness can be obtained as:

$$\frac{\partial \delta}{\partial t} = -\left\{ \frac{k_l (T_W - T_{SAT})}{\rho_l h_{fg}} \right\} \frac{1}{\delta(r,t)} \tag{5}$$

By separating variables and integrating this equation we arrive at an expression for the transient evolution of the local microlayer thickness:

$$\delta(r,t) = \sqrt{(\delta_0(r))^2 - \frac{2k_l (T_W - T_{\text{int}})}{\rho_l h_{fg}} t} \tag{6}$$

where $\delta_0(r) = \delta(r, t = 0)$ is the radial variation of initial microlayer thickness.

However, the wall temperature does change rapidly both radially and in time, in response to the resulting evaporative wall heat flux $\dot{q}''_W = q''_{EV}$. We will return to this point in Section 3.3.

Parameters upon which the results of this type of sub-grid model depend are the initial microlayer thickness, and in particular the variation of this thickness as the radial extent of the microlayer increases with the bubble growth. Parameters representing this are selected based on such (limited) quantified experimental evidence as is available for the case being studied, and they are quantities that are challenging to measure. For much of the parameter space microlayer-induced growth is a dominant part of total bubble growth predicted. The values chosen for the open parameters in practice then play a role in determining the overall predicted bubble growth, which is not ideal and leaves much scope for future research.

3.2.3. Comparison

'Triple line' and 'whole microlayer' models show significantly different vapour production rates. Fundamentally this is due to the fact that the triple-line and the whole-microlayer cover very different amounts of the substrate's surface area.

Experimental observations at atmospheric pressure conditions consistently show a cooling of the substrate surface underneath steam bubbles beyond the triple line region and up to radial lengths of a few millimetres (Gerardi et al., 2010; Kim and Buongiorno, 2011; Duan et al., 2013). These experiments confirm that the modelling of an enhanced mass transfer solely in the triple line region is not sufficient to represent accurately the physics underneath a bubble growing at atmospheric pressure conditions. The typical temporal evolution of the dryout radius and outer radius of the microlayer for sequential steam bubbles under atmospheric pressure as measured by Jung and Kim (2015) is illustrated in Fig. 10. These measurements allow us to plot approximate dry patch, contact line and microlayer areas versus time. The comparison in Fig. 10 shows that the triple line area is generally very small compared to the extended microlayer region, which covers the major part of the area underneath the bubble for most of the ebullition time. Supported by such experimental data, the current trend is to the modelling of the heat transfer and vapour generation underneath steam bubbles at atmospheric pressure via the more accurate 'whole' microlayer models.

3.3. The importance of conjugate heat transfer

With the high heat fluxes predicted at the wall, it is likely that the wall surface temperature will be caused to fall, and thermal diffusivity within the substrate will exert a significant influence on heat transfer and evaporation. We will now move to an investigation of this.

3.3.1. Approximate analysis

As discussed, the physical foundation of the basic microlayer evaporation model consists of simple heat conduction through the liquid layer, such that the layer evaporates until it is wholly depleted. The local heat flux is given by Eq. (4). Typical average dimensions of a microlayer, substrate properties and conditions are listed in Table 6.

Using the microlayer dimensions in Table 6, we can estimate a typical wedge-shaped microlayer volume to be initially:

$$\bar{V}_{ML} = \frac{2}{3} \pi R^2 \delta_{\max} \tag{7}$$

The recent experimental data of Jung and Kim (2014) suggests that the entire microlayer is evaporated within ~10 ms, before the bubbles leave the wall. If we take this time period over which to evaporate the entire microlayer volume an average wall heat flux, based on measurements, is obtained:

$$\bar{\dot{q}}'' = \frac{2}{3} \frac{\delta_{\max} \rho_l}{\tau} \Delta h_{fg} \tag{8}$$

The average heat flux calculated from Eq. (8) with the values given in Table 6 is ~600 kWm^{-2}. Even though on a real heater surface local wall heat fluxes change significantly during an ebullition cycle, this average flux agrees well with the experimental observations of Jung and Kim (2014), who measured wall heat fluxes between 400–900 kWm^{-2}.

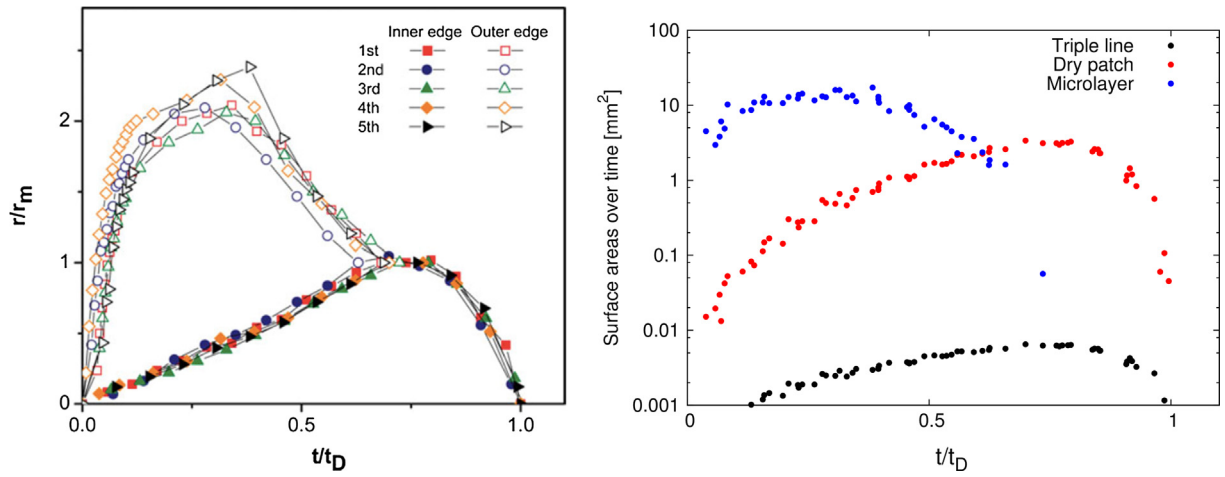

Fig. 10. Temporal evolution of the radius of the contact-line and the outer radius of the microlayer, taken from Jung and Kim (2015) (left); and the corresponding evolution of the area of the dry patch, of the contact-line, and of the microlayer over time (right).

Table 6
Characteristic microlayer dimensions and sapphire substrate properties.

Microlayer quantities		
Maximum thickness (δ_{max})	μm	4
Radial extent (R)	μm	1000
Bubble ebullition period	ms	15
Microlayer evaporation period	ms	10
Nominal wall superheat	K	10
Sapphire properties		
Substrate specific heat	J kg^{-1} K^{-1}	900
Substrate thermal conductivity	W m^{-1} K^{-1}	30
Substrate density	kg m^{-3}	3970

As a simple model by which to assess the effect this has on the wall surface temperature, we will consider a semi-infinite solid (sapphire, typical of experimental arrangements) of uniform initial temperature subject to this heat flux for some time period τ. From Carslaw and Jaeger (1959), the reduction in wall surface temperature is given by:

$$T_W(\tau) - T_W(0) = -\frac{2\bar{q}''}{k_s}\sqrt{\frac{k_s}{\pi\rho_s c_{p,s}}\tau} \quad (9)$$

We will apply the heat flux of 600 kWm^{-2}, as calculated above, into Eq. (9) up to the time when the microlayer has been depleted. The associated surface temperature variation is shown in Fig. 11, where a temperature drop of 4–5 K can be observed caused by microlayer depletion.

Cooper and Lloyd (1969) derived an analytical expression for the evaporated volume from the liquid microlayer as a function of time assuming ideal hemispherical bubble growth according to the correlation of Plesset and Zwick (1954). This allows us to plot the integrated mass transfer rate over time from the microlayer, with and without the influence of conjugate heat transfer into the solid. This is illustrated in Fig. 12. Further details can be found in Hänsch et al. (2015).

The solid, black line in Fig. 12 represents the mass transfer rate required for a bubble to grow at the rate that it would need if it were an ideal hemisphere. The coloured lines illustrate the area-integrated mass transfer rates from microlayer evaporation with a constant wall temperature, and with conjugate heat transfer. The comparison shows that the integrated mass transfer rate can drop significantly when the substrate surface temperature drop is taken into account. The evaporation rate using typical microlayer dimensions drops to about 50% of the isothermal-substrate case.

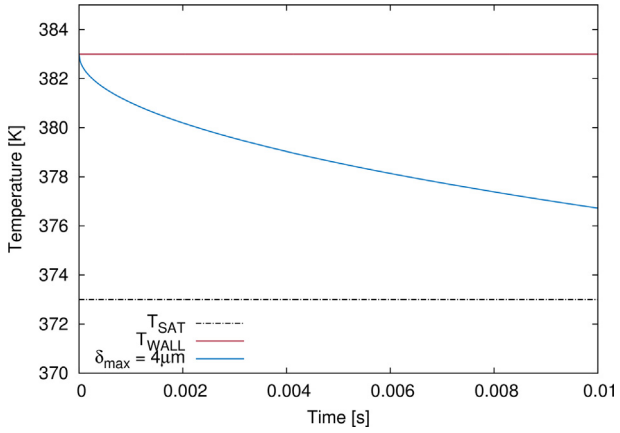

Fig. 11. The variation of surface temperature reduction with time for an average heat flux of 600 kWm^{-2} (1 mm × 4 μm microlayer evaporating over 10 ms).

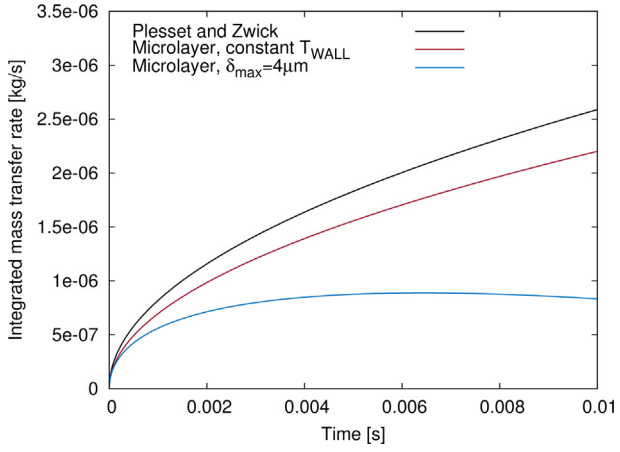

Fig. 12. Total vapour volume produced by the microlayer model over time for a constant wall temperature (red line), and for a variable surface temperature according to the evaporation of an idealized microlayer wedge (blue line). (For interpretation of the references to colour in this figure legend, the reader is referred to the web version of this article.)

The comparison confirms that microlayer evaporation models should not be employed without considering the cooling of the solid underneath. The thermal response of the heater to the microlayer evaporation should be an integral part of the simulations.

3.3.2. Computational analysis

The above analytical investigation of the significance of conjugate heat transfer for the microlayer evaporation is here extended by computational investigations using the interface-tracking code TransAT. A sub-grid model for microlayer evaporation has been developed and paired with conjugate heat transfer. Simulations with conjugate heat transfer and a pseudo-Dirichlet boundary condition allow us to investigate the behaviour with and without a thermally-coupled substrate.

As a test case we attempt to analyse a nucleate boiling experiment performed by Duan et al. (2013) at atmospheric pressure. The heated wall consists of a 0.25 mm thick sapphire substrate (with properties listed in Table 6) to which an input heat flux of 28.7 kWm^{-2} was provided via a thin Indium-Tin Oxide layer on the wetted side. Note that the heat is generated within a layer much thinner than the thermal penetration depth noted above, which is not fully consistent with the analytical model adopted, but as the transient local heat flux extracted is more than an order of magnitude greater than the average heat generation rate applied, the conclusions will be unaltered.

The computational domain was specified as 6 mm in the horizontal and 10 mm in the vertical directions. A 2D axisymmetric model was employed.

For the top of the domain an outflow boundary condition was applied, whilst for the sides symmetry was imposed. For the contact-line between vapor, liquid and solid a static apparent contact angle of 40° was applied as observed in the experiments. Initially, the entire domain is assumed to be at rest with a wall thermal boundary layer thickness evaluated from the correlation for turbulent natural convection heat transfer (Kays and Crawford, 1980):

$$\delta_T = 7.14\sqrt[3]{\frac{\upsilon_l \alpha_l}{g\beta_T \Delta T}} \tag{10}$$

For the simulation with a pseudo-Dirichlet boundary condition a heater region was modelled. This region was extremely thin, and was ascribed a conductivity 50 times higher than the actual sapphire substrate, such that the underside of the water was maintained, to within a fraction of a degree, at the temperature of the underside of the substrate.

For the conjugate heat transfer case the substrate was given a uniform initial temperature, at the superheated wall temperature. It was heated by a heat flux applied to the underside of the substrate. Given the short period simulated, this heat flux plays little role.

In Fig. 13 the bubble dimensions (bubble base diameter, height, maximum lateral dimension and bubble equivalent diameter) computed with both the pseudo-Dirichlet and the conjugate heat transfer boundary conditions, are plotted and compared over time. A significant change of bubble growth rate can be observed. The pseudo-Dirichlet boundary condition generally produces bubble radii twice those predicted when conjugate heat transfer is included.

Fig. 14 shows two snapshots of the bubble simulation with the conjugate heat transfer included. We can see the dry patch is growing radially outwards as the microlayer is depleted over time. The bubble shape is changing from oblate to nearly spherical by the time of departure.

Fig. 15 illustrates the evaporative mass transfer rates for the two cases, with the mass transfer subdivided into the contributions of phase change from the curved surface and the microlayer evaporation. The results for the pseudo-Dirichlet boundary condition show that most of the bubble growth can be attributed to the

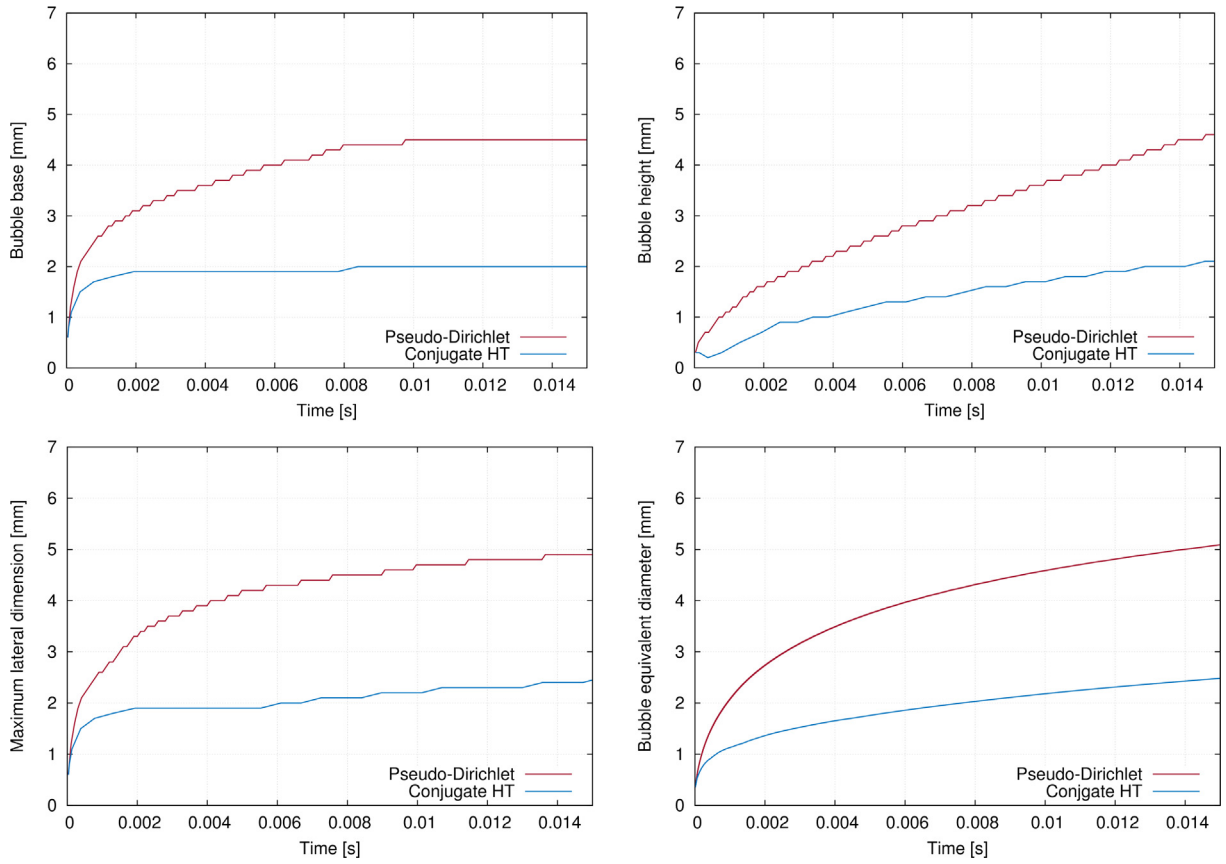

Fig. 13. Comparison of predicted bubble dimensions with Dirichlet and conjugate heat transfer boundary condition at the wall.

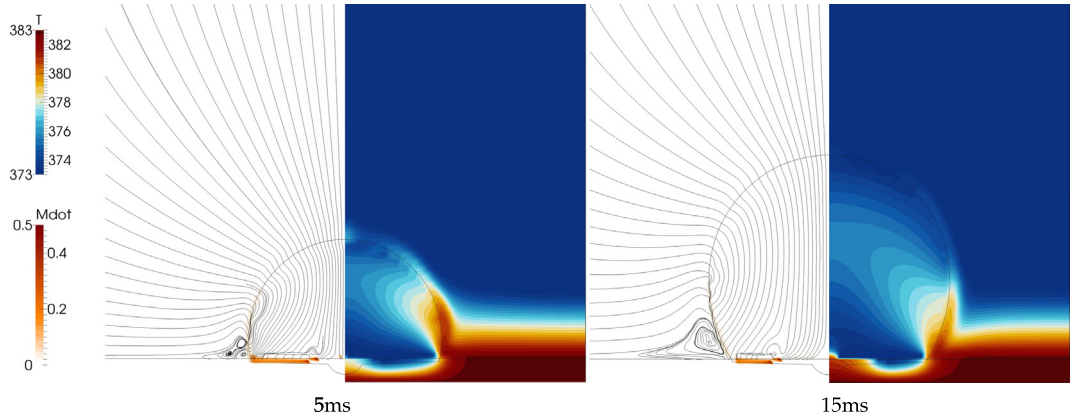

Fig. 14. Streamline plots, mass transfer rates and temperature fields after 5 ms and 15 ms (image excerpts of 3 mm radial extent and 4.73 mm height).

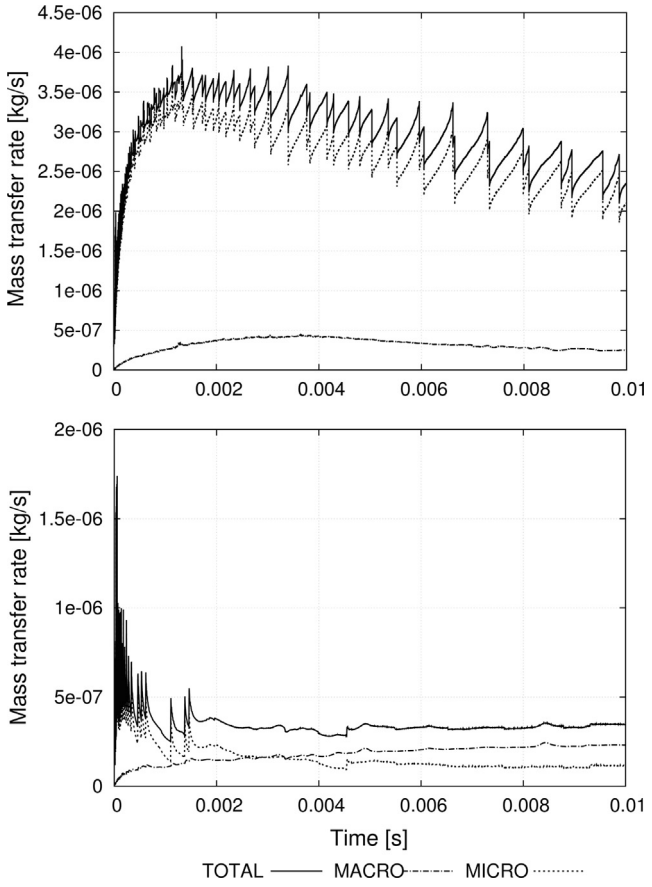

Fig. 15. Comparison of the mass transfer rates (total and contributions from the curved surface and the microlayer). Top: pseudo-Dirichlet. Bottom: conjugate heat transfer.

microlayer evaporation. Note that for this study only a single bubble is investigated. For subsequent bubbles the contribution of the curved surface will change due to the establishment of a quasi-steady thermal boundary layer over time. The results in Fig. 15, using the initial convective thermal boundary layer according to Eq. (10), nonetheless demonstrate the significance of the microlayer contribution to the overall bubble growth.

The cooling of the substrate markedly decreases the microlayer heat flux and associated mass transfer rate, as illustrated at the bottom of Fig. 15. The production of vapour from the microlayer is grossly over-predicted when applying a constant wall temperature. The great importance of microlayer evaporation compared to evaporation from the curved surface, however, remains clear.

3.4. Evaporative thermal resistance

Microlayer evaporation models, as described above, model the process of evaporation at the interface as 'perfect' in the sense that there is no restriction to vapour generation, and the interface is taken to be at the saturation temperature. However, very high heat fluxes through the microlayer have been measured, so that kinetic effects and the associated evaporative thermal resistance need to be considered in modelling of microlayer depletion (Giustini et al., 2016). For the 'older' triple line models the evaporative thermal resistance was indeed generally taken into account, given the even thinner films and higher heat fluxes considered there.

The work of Utaka et al. (2013) was the first to consider including evaporative thermal resistance into the evaporation model of a 'whole' microlayer, as it was expressed in Eq. (2). The evaporative heat transfer coefficient is expressed as:

$$h_{evap} = \frac{2\alpha}{2-\alpha}\frac{h_{fg}^2 \rho_v}{\sqrt{2\pi R_{gas}} T_{sat}^{\frac{3}{2}}} \tag{11}$$

In the above expression the vital parameter is α, the 'accommodation coefficient'. (It should be pointed out that other authors refer to $f = 2\alpha/(2-\alpha)$ as the accommodation coefficient.) Broadly, for evaporation, it is a measure of the fraction of molecules that escape from the liquid, and successfully remain in the vapour, rather than 'bounce' back into the liquid. Utaka et al. (2013) caused evaporative thermal resistance to have little effect on the evaporation rate (via the assumption of an accommodation coefficient ~0.5), and it was ignored in further analysis.

A more recent study by Giustini et al. (2016) shows that evaporative thermal resistance can play a major role in heat transfer through the microlayer under atmospheric steam-water conditions. The analysis of experimental data from Jung and Kim (2015) suggests accommodation coefficient values between 0.01 and 0.1.

Both conduction through the microlayer and evaporative thermal resistance at the liquid–vapour interface may be of great importance to phase change within the microlayer. We will investigate their relative importance by plotting the magnitude of each component separately. The evaporative thermal resistance is represented by a constant that solely depends on material properties and the choice of the accommodation coefficient:

$$R_{EVAP} = \frac{1}{h_{evap}} \tag{12}$$

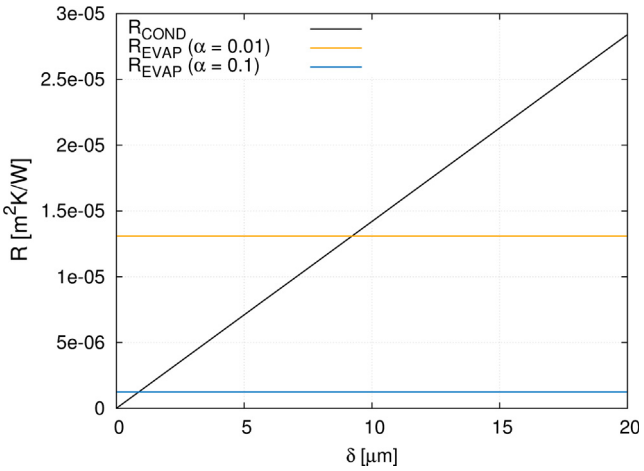

Fig. 16. Thermal resistances for different microlayer thicknesses.

The conductive resistance depends on the thickness of the liquid layer through which the heat has to flow

$$R_{COND} = \frac{\delta}{k_l} \tag{13}$$

Fig. 16 compares the value of the evaporative resistance with accommodation coefficients between 0.01 and 0.1 with the conductive resistance for different microlayer thicknesses.

Typical initial microlayer thicknesses have been measured to be around ~4 μm and during the bubble growth process the liquid film depletes rapidly. The comparison in Fig. 16 shows that for such microlayer thicknesses the inclusion of an evaporative thermal resistance may become necessary, but the contribution of such resistance depends on the value of the accommodation coefficient believed appropriate. As noted, recent experimental measurements indicate that values in the range 0.01–0.1 may be applicable under these conditions. Given the rapid evaporation of the liquid films to thicknesses far below ~4 μm, the inclusion of some representation of evaporative thermal resistance seems needed.

4. Microlayer formation

4.1. Introduction

We have seen above the important role that the microlayer plays in the growth, in particular, of atmospheric pressure bubbles. We also noted that the results of microlayer evaporation models depend on input parameters describing the initial microlayer dimensions, based upon a rather sparse set of experimental observations.

In this section we present very briefly a summary of some recent work that attempts to model the hydrodynamics of the formation of microlayers for steam-water bubbles at atmospheric pressure conditions.

Further details are available in a conference paper (Hänsch and Walker, 2016b), and in a recent journal submission (Hänsch and Walker, 2016a).

Only the hydrodynamics of the formation, with no modelling of any phase change, are considered. It was felt prudent to gain a clearer idea of the physical processes determining the basic formation before incorporating the considerable additional complexities associated with the rapid evaporation of the layer as it is formed.

In order to be sure a physically plausible bubble growth rate was used, we took the analytical solution of Scriven (1959) and from that determined essentially a vapour volumetric generation rate (per unit area) as function of time. This generation rate was then applied to the growing curved surface of the bubble.

As will be apparent from the discussion of microlayer and bubble dimensions above, considerable mesh refinement is needed to resolve velocity fields within the thickness of the microlayer itself. That generates additional difficulties because of the consequent requirements for an extremely small time-step in order to satisfy Courant limits for stability.

In Fig. 17 we show the computational domain and mesh employed, for the series of analyses with three different growth rates characterised in Table 7. The achievement of mesh

Table 7
The three sets of growth rates studied, characterised by the superheats used in the Scriven calculation from which the vapour generation rate was determined.

	Rate 1	Rate 2	Rate 3
Parameters			
Scriven ΔT (K)	5	10	15
Ja number	15.44	30.94	46.4
Rtrans (μm)	25	72	132
Simulation specifications			
Seed size (μm)	30	80	140
Initial time (μs)	5.94	10.8	14.85
Initial mdot (kg/m² s)	1.46	2.14	2.73

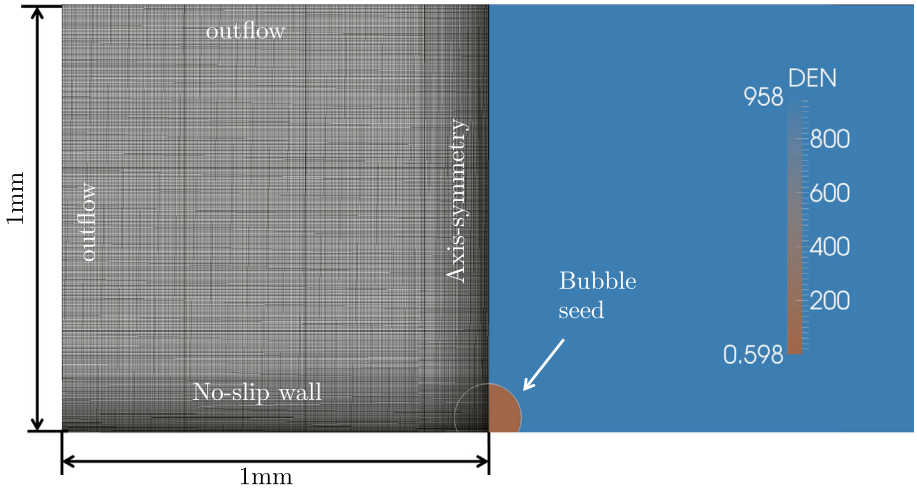

Fig. 17. Computational domain and boundary conditions for the microlayer formation simulation.

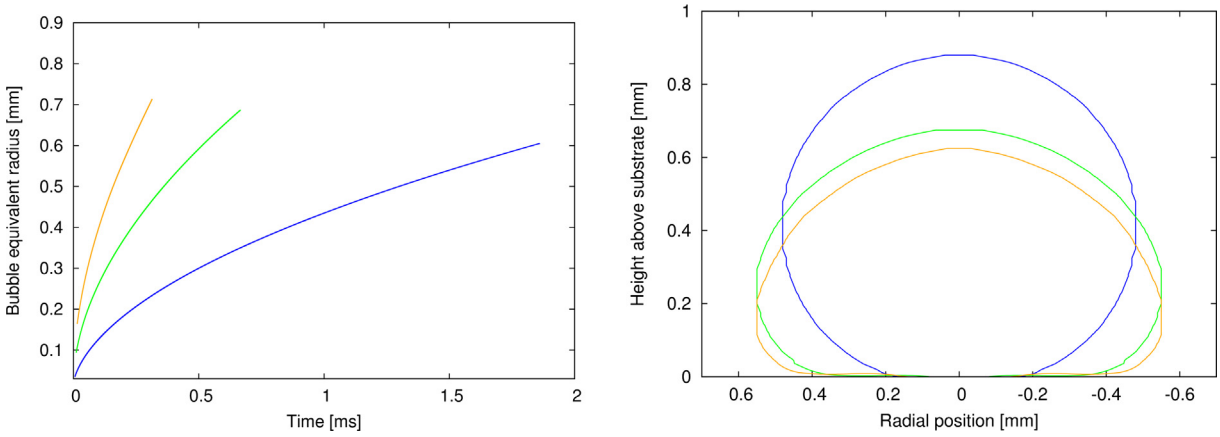

Fig. 18. Left: computed bubble equivalent radius over time for different mass transfer rates (Blue: Rate1, Green: Rate 2, Yellow: Rate 3). Right: bubble shapes for the same bubble equivalent diameter after different times (Rate 1: 1.83 ms, Rate 2: 0.51 ms, Rate 3: 0.23 ms). (For interpretation of the references to colour in this figure legend, the reader is referred to the web version of this article.)

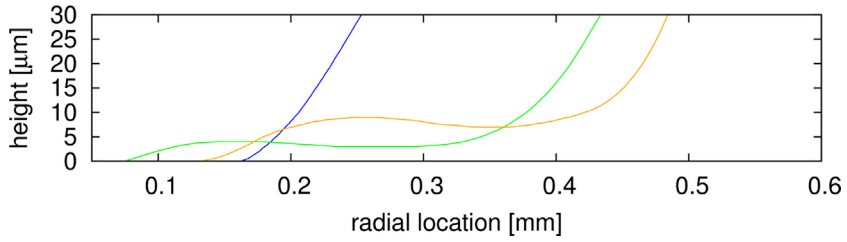

Fig. 19. Microlayer outlines for the different bubble growth rates at different times. Blue: Rate 1 at 1.84 ms, Green: Rate 2 at 0.5 ms, Yellow: Rate 3 at 0.23 ms. (For interpretation of the references to colour in this figure legend, the reader is referred to the web version of this article.)

independence, and other more detailed aspects of the modelling, are discussed in the full paper cited earlier.

4.2. Bubble shape and microlayer extent

Fig. 18 shows clearly that for the lower growth rate the bubble retains a more or less spherical form, with only a limited near-flat region close to the substrate. As the bubble growth rate increases, the bubble becomes increasingly oblate, with a progressively wider microlayer trapped as the vapour advances.

This is seen in rather more detail in Fig. 19 where the microlayer from these three cases is shown in a close up view

Some recent experimental results of Jung and Kim (2014) are shown in Fig. 20, along with simulations at a slightly higher growth rate than Rate 3, selected so as to match the growth rate in bubble volume observed in the experiment.

We see that whilst there is something of a gap in shape observation near the wall, the general form of the interface, and e.g. the increase in microlayer extent with time, is well predicted.

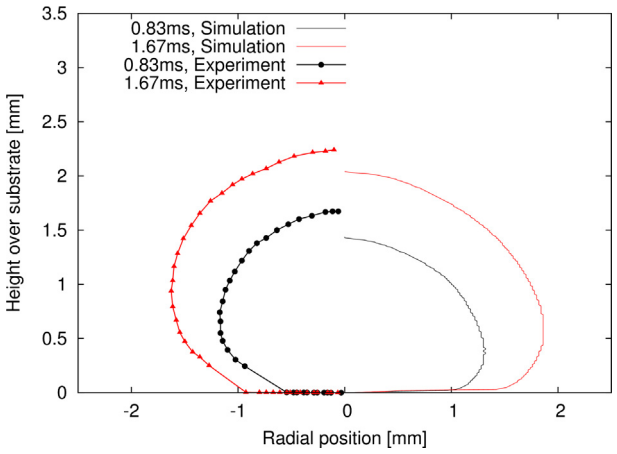

Fig. 20. Bubble shapes compared to the experimental observations of Jung and Kim (2014).

4.3. The causes of microlayer formation

Macroscopically, where a bubble's shape lies between spherical and hemispherical largely depends on the balance between the surface tension which is attempting to force it to be spherical, and the force required to overcome the inertia of the surrounding fluid that needs to be displaced for the bubble to grow.

With higher growth rates (and, indeed, although the results are not shown here, with reduced surface tension), the bubble tends to be more hemispherical and to exhibit a greater radial extent of microlayer. This seems to be the main determinant of the existence and then radial extent of the microlayer.

When a microlayer is formed, its thickness seems largely to be determined as a result of the radially-outward motion of the interface, caused by the evolving vapour, which is resisted by the liquid in contact with the surface, and subject to a no-slip condition there.

4.4. Closing remarks

Recall, the above analyses addressed purely the hydrodynamics. That causes the prediction of a relatively thick microlayer; the evaporation discussed above in this paper actually causes the

thickness to reduce very rapidly. Indeed, such experimental measurements as there are of microlayer thicknesses show them to be significantly smaller than predicted here, but this is to be expected. Obviously, the next step is to take this hydrodynamics-only model, and incorporate into it an appropriate mechanistic phase change model to try to form a composite self-consistent physical model of the formation and depletion of the microlayer.

5. Conclusions

We have here summarised much of the recent work in the area of interface-tracking computations of single bubble growth within the NURESAFE project.

In summary: Our implementation of the phase change at the interface between the two fluids is currently under further development. Proper evaluation requires a mesh fine enough to resolve the very local unsteady temperature distribution in the surrounding superheated liquid. This very fine mesh can in turn result in spurious parasitic currents. These are a wholly numerical aberration, and known means to overcome this are being implemented. Along with this a more advanced phase change model itself is desirable, and a prototype version is already implemented in a pre-release version of the code.

Certainly for atmospheric pressure bubbles, much of the growth of the bubble is caused by the rapid evaporation of the microlayer, the thin-layer "left behind" as the bubble expands over the surface of the heated substrate. The fact that this layer is so thin itself makes the modelling of its evaporation, generally done via sub-grid models, rather troublesome. Rates of heat transfer are such that conjugate heat transfer and transient local cooling within the heated solid substrate cannot be neglected. Similarly, evaporative processes can normally be assumed to offer negligible resistance to the flow of heat, compared to the other thermal resistances, in engineering devices. Here, however, the conductive resistance of the vanishingly thin microlayer is so small that it seems that evaporative resistance is likely to be significant. This needs to be incorporated in microlayer evaporation models in the future.

The great importance of the microlayer in bubble formation, and the great sensitivity of the rate of bubble growth to the microlayer dimensions, has encouraged us to attempt to understand the process of microlayer formation more mechanistically, rather than rely upon the (understandably) very sparse set of experimental measurements of microlayer dimensions. We have here presented mechanistic simulations of the growth of microlayers, which display characteristics that are consistent with such observations as we have. They suggest that the main determinant of the existence and extent of a microlayer (for a given fluid) is the rate of bubble growth, with rapid bubble growth being such that an oblate sphere is generated, and then viscous effects beneath it mean that the liquid cannot be dragged away, but rather leaves behind the microlayer.

Work on augmenting and extending this microlayer hydrodynamic treatment to include heat and mass transfer is currently in hand.

Acknowledgements

The work is supported by EPSRC in collaboration with ASCOMP AG and the NURESAFE project. It is a pleasure to acknowledge helpful discussions with Giovanni Giustini, Ronak Thakrar, Frederic Sebilleau and Keith Ardron, all of Imperial College London.

References

ASCOMP 2015. TransAT Handbook Series. Multiphase Flow Modelling.

Carslaw, H.S., Jaeger, J.C., 1959. Conduction of Heat in Solids. Oxford University Press.

Chen, Z., Utaka, Y., 2015. On heat transfer and evaporation characteristics in the growth process of a bubble with microlayer structure during nucleate boiling. Int. J. Heat Mass Transfer 81, 750–759.

Cooper, M.G., Lloyd, A.J.P., 1969. The microlayer in nucleate pool boiling. Int. J. Heat Mass Transfer 12, 895–913.

Delgoshaei, P., 2009. Microscale heat transfer measurements during subcooled pool boiling of pentane: effect of fluid properties and bubble dynamics (Ph.D.). University of Maryland.

Duan, X., Phillips, B., Buongiorno, J., 2013. Synchronized high-speed video, infrared thermometry, and particle image velocimetry data for validation of interface-tracking simulations of nucleate boiling phenomena. Exp. Heat Transfer 26, 169–197.

Fath, H.S., Judd, R.L., 1978. Influence of system pressure on microlayer evaporation heat transfer. J. Heat Transfer 100, 49–55.

Fuchs, T., Kern, J., Stephan, P., 2006. A transient nucleate boiling model including microscale effects and wall heat transfer. J. Heat Transfer 128, 1257–1265.

Gerardi, C., Buongiorno, J., Hu, L.-W., McKrell, T., 2010. Study of bubble growth in water pool boiling through synchronized, infrared thermometry and high-speed video. Int. J. Heat Mass Transfer 53, 4185–4192.

Gibou, F., Chen, L., Nguyen, D., Banerjee, S., 2007. A level set based sharp interface method for the multiphase incompressible Navier-Stokes equations with phase change. J. Comput. Phys. 222, 536–555.

Giustini, G., Jung, S., Kim, H., Walker, S., 2016. Evaporative thermal resistance and its influence on microscopic bubble growth. Int. J. Heat Mass Transfer 101, 733–741.

Guion, A., Langewisch, D., Buongiorno, J., 2013a. Dynamics of the liquid microlayer underneath a vapor bubble growing at a heated wall. Summer Heat Transfer Conference. Minneapolis, MN, USA.

Guion, A., Rabello Dos Anjos, G., Narayanan, C., Buongiorno, J., 2013b. Closure Relation for Microlayer Evaporation in Nucleate Boiling, and its Application to ITM Test Case 3b.

Hänsch, S., Narayanan, C., Reboux, S., Giustini, G., Walker, S., 2015. Microlayer models for nucleate boiling simulations: the significance of conjugate heat transfer. NURETH-16. Chicago.

Hänsch, S., Walker, S., 2016a. The hydrodynamics of microlayer formation beneath vapour bubbles. Int. J. Heat Mass Transfer 102, 1282–1292.

Hänsch, S., Walker, S., 2016b. The hydrodynamics of the formation of microlayers beneath vapour bubbles growing on a heated substrate. ATH-16. New Orleans.

Jung, S., Kim, H., 2014. An experimental method to simultaneously measure the dynamics and heat transfer associated with a single bubble during nucleate boiling on a horizontal surface. Int. J. Heat Mass Transfer 73, 365–375.

Jung, S., Kim, H., 2015. An experimental study on heat transfer mechanisms in the microlayer using integrated total reflection, laser interferometry and infrared thermometry technique. Heat Transfer Eng. 36, 1002–1012.

Kays, W.M., Crawford, M.E., 1980. Convective Heat and Mass Transfer, New York.

Kim, H., Buongiorno, J., 2011. Detection of liquid–vapor–solid triple contact line in two-phase heat transfer phenomena using high-speed infrared thermometry. Int. J. Multiphase Flow 37, 166–172.

Koffmann, L.D., Plesset, M.S., 1983. Experimental observations of the microlayer in vapor bubble growth on a heated solid. J. Heat Transfer 105, 625–632.

Kunkelmann, C., Stephan, P., 2009. CFD simulation of boiling flows using the volume-of-fluid method within OpenFOAM. Numer. Heat Transfer Part A 56, 631–646.

Langewisch, D., 2012. Areva Doctoral Fellowship Final Report. Massachusetts Institute of Technology.

Lay, J.H., Dhir, V.K., 1995. Shape of a vapor stem during nucleate boiling of saturated liquids. J. Heat Transfer 117, 394–401.

Moore, F.D., Mesler, R.B., 1961. The measurement of rapid surface temperature fluctuations during nucleate boiling of water. AIChE J. 7, 620–624.

Moosman, S., Homsy, G.M., 1980. Evaporating menisci of wetting fluids. J. Colloid Interface Sci. 73, 212–223.

Plesset, M.S., Zwick, A., 1954. The growth of vapour bubbles in superheated liquids. J. Appl. Phys. 25, 493-450.

Sakashita, H., 2011. Bubble growth rates and nucleation site densities in saturated pool boiling of water at high pressures. J. Nucl. Sci. Technol. 48, 734–743.

Sato, Y., Ničeno, B., 2015. A depletable micro-layer model for nucleate pool boiling. J. Comput. Phys. 300, 20–52.

Schrage, R.W., 1953. A Theoretical Study of Interphase Mass Transfer. Columbia University Press, New York.

Scriven, L.E., 1959. On the dynamics of phase growth. Chem. Eng. Sci. 10, 1–13.

Sharp, R.R., 1964. The Nature of Liquid Film Evaporation during Nucleate Boiling. NASA.

Snyder, N.R., Edwards, D.K., 1956. Summary of Conference on Bubble Dynamics and Boiling Heat Transfer. Jet Propulsion Laboratory.

Son, G., Dhir, V.K., Ramanujapu, N., 1999. Dynamics and heat transfer associated with a single bubble during nucleate boiling on a horizontal surface. J. Heat Transfer 121, 623–631.

Stephan, P., Hammer, J., 1994. A new model for nucleate boiling heat transfer. Wärme- und Stoffübertragung 30, 119–125.

Stephan, P.C., Busse, C.A., 1992. Analysis of the heat transfer coefficient of grooved heat pipe evaporator walls. Int. J. Heat Mass Transfer 35, 383–391.

Utaka, Y., Kashiwabara, Y., Ozaki, M., 2013. Microlayer structure in nucleate boiling of water and ethanol at atmospheric pressure. Int. J. Heat Mass Transfer 57, 222–230.

Utaka, Y., Kashiwabara, Y., Ozaki, M., Chen, Z., 2014. Heat transfer characteristics based on microlayer structure in nucleate pool boiling for water and ethanol. Int. J. Heat Mass Transfer 68, 479–488.
Wang, H., Garimella, S.V., Murthy, J.Y., 2007. Characteristics of an evaporating thin film in a microchannel. Int. J. Heat Mass Transfer 50, 3933–3942.
Wang, H., Garimella, S.V., Murthy, J.Y., 2008. An analytical solution for the total heat transfer in the thin-film region of an evaporating meniscus. Int. J. Heat Mass Transfer 51, 6317–6322.
Wayner, P.C., Kao, Y.K., Lacroix, L.V., 1976. The interline heat-transfer coefficient of an evaporating wetting film. Int. J. Heat Mass Transfer 19, 487–492.
Yabuki, T., Saitoh, T., Nakabeppu, O., 2013. Contribution of microlayer evaporation to bubble growth in pool saturated boiling of water. ASME 2013 11th International Conference on Nanochannels, Microchannels, and Minichannels. Sapporo, Japan.